


## Shell model and Hartree-Fock calculations of longitudinal and transverse electroexcitation of positive and negative parity states in $^{17}\text{O}$

Ali A. Alzubadi,\* R. A. Radhi, and Noori S. Manie

*Department of Physics, College of Science, University of Baghdad, Baghdad, Iraq*

 (Received 4 October 2017; revised manuscript received 23 December 2017; published 15 February 2018)

The nuclear structure of the  $^{17}\text{O}$  nucleus has been investigated using shell model and self-consistent Hartree-Fock calculations. In particular, elastic and inelastic electron scattering form factors, energy levels, and transition probabilities are calculated for positive and negative low-lying states. Two different shell model spaces have been used for this purpose. The first one is the *psd<sub>pn</sub>* model space for positive parity states and the second one is *p<sub>1/2</sub>sd* model space for negative parity states. For all selected excited states, Skyrme interactions are adopted to generate from them a one-body potential in Hartree-Fock theory to calculate the single-particle matrix elements. The deduced results are discussed for the longitudinal and transverse form factors and compared with the available experimental data. It has been confirmed that combining the shell model plus Hartree-Fock mean field method with the Skyrme interaction can accommodate very well the nuclear excitation properties, and work better for low lying states than for higher excitations. Furthermore, the combination can be used to reproduce the positive and negative parity states after choosing the suitable model space, effective two-body interaction, and parameterization to reach highly descriptive and predictive results.

DOI: [10.1103/PhysRevC.97.024316](https://doi.org/10.1103/PhysRevC.97.024316)

### I. INTRODUCTION

The study of nuclear structure is usually performed with two major approaches: the well-established shell model (SM) and the self-consistent mean-field (SCMF) method. Both approaches work at a microscopic level but employ effective interactions to allow a treatment in either restricted spaces or forms of many body wave functions [1].

The SM techniques with empirical interactions can be applied to many regions of the nuclear chart, including exotic nuclei, with great success in a detailed description of their spectroscopy and decays. In contrast to the mean-field techniques, the SM does not involve a single, global Hamiltonian for the whole nuclear chart. Furthermore, the SCMF has a wide applicability across the nuclear chart in evaluating the ground state nuclear properties, for instance the binding energy, nuclear size, form factors, and surface deformation parameters. However, it does not give detailed spectra of excited states and wave functions. The SCMF is based on an independent particle picture, where the nucleons are considered to be self-bound by the average of the two-body interactions over the states occupied by the other particles. The resulting field is created in a self-consistent manner. Such a field is considered to be static, so that dynamical corrections are neglected. Specifically, this approach can be realized by means of an adopted effective interaction, solved at the level of the Hartree-Fock (HF) approximation.

The SM allows for configuration mixing (CM) beyond the mean field [2], so one can take for the mean field a standard phenomenological single-particle model, but then perform a CM calculation involving all many-body states that can be

constructed using a more or less broad band of single-nucleon states around the Fermi energy [3].

In the present work, we continue our research [4] into applying the SM and HF approaches in calculating the inelastic electron scattering form factors for positive and negative parity states in the  $^{17}\text{O}$  nucleus. The nucleus  $^{17}\text{O}$  is known to have approximately 112 excited states below 24 MeV energy of excitation [5]. This nuclear system presents an interesting opportunity to understand some rich excited levels in a light, stable nucleus. Numerous experimental and theoretical studies have been performed to investigate the static and dynamic nuclear properties of this interesting nuclear system. Arnke [6] employed the SM calculations to evaluate the energy levels for lowest parity states  $1/2^-$  and  $3/2^-$  in  $^{17}\text{O}$ . Hicks [7] calculated the  $M1$  and  $M3$  form factors and the root-mean-square (rms) radius of the  $1d_{5/2}$  neutron orbit of  $^{17}\text{O}$ . Quantitative information on the quenching of the  $M3$  and  $M5$  multipoles was also deduced.

Elastic magnetic electron scattering from  $^{17}\text{O}$  was studied by G. Bohannon *et al.* using spherical and deformed mean field models taking into account core polarization effects, for the first time [8]. Elastic charge and magnetic form factors of  $^{17}\text{O}$  were calculated by Kim [9] using a consistent relativistic formalism for momentum transfers up to  $7.5\text{ fm}^{-1}$ . Excited states of  $^{17}\text{O}$  up to the excitation energy of 15 MeV were studied by Manley *et al.* [10] using high-resolution electron scattering for momentum transfers between  $0.8$  and  $2.6\text{ fm}^{-1}$ . Gattone and Vary [11] studied the elastic magnetic form factor of  $^{17}\text{O}$  using the relativistic direct-interaction-based impulse approximation model. Coon and Jaqua [12] determined the parameters of an algebraic radial wave function corresponding to the  $1d_{5/2}$  valence neutron orbital of  $^{17}\text{O}$  by making a fit to the high- $q$  magnetic electron scattering data. Zheng *et al.* [13] calculated the elastic magnetic form factor of  $^{17}\text{O}$  by

\*Corresponding author: [ali.a.alzubadi@scbaghdad.edu.iq](mailto:ali.a.alzubadi@scbaghdad.edu.iq)

including the  $2\bar{h}\omega$  particle-hole excitation and the Zuker-type multiparticle-multihole CM in the momentum transfer range  $0.5 - 1.5 \text{ fm}^{-1}$ . Shell model and deformed HF plus Bardeen-Cooper-Schrieffer (BCS) calculations for even-even isotopes  $^{18-30}\text{O}$  were reported by Siiskonen *et al.* [14]. Ground-state binding energies and  $2_1^+$  quadrupole moments are calculated by both models. Radhi *et al.* [15] investigated the elastic magnetic electron scattering form factors for the  $5/2^+$  state of the stable odd- $A$  nuclei including  $^{17}\text{O}$  in the  $sd$  shell, taking into consideration core polarization effects.

Our concern in the present work is to calculate the elastic and inelastic longitudinal and transverse electron scattering form factors for positive and negative parity states in the  $^{17}\text{O}$  nucleus. Two different model spaces are used for this purpose. The first one is the  $psdnpn$  model space for positive parity states, which consists of the active shells  $1p_{1/2}$ ,  $1p_{3/2}$ ,  $1d_{3/2}$ ,  $1d_{5/2}$ , and  $2s_{1/2}$  above the inert  $^4\text{He}$  nucleus core  $(1s)^4$ , which remains closed. The interaction used is the PSDMOD Hamiltonian [16] which has been used to provide realistic  $psdnpn$ -shell wave functions for the positive parity states  $1/2^+$  0.8707 MeV,  $1/2_2^+$  6.356 MeV,  $1/2_3^+$  7.956 MeV,  $3/2^+$  5.084 MeV,  $3/2_2^+$  5.869 MeV,  $5/2^+$  6.862 MeV,  $5/2_3^+$  8.402 MeV,  $7/2^+$  7.576 MeV, and  $9/2^+$  8.470 MeV. In this Hamiltonian, the multiparticle-multihole states around  $^{16}\text{O}$  are accounted for by reproducing the correct binding energy relative to the  $^{16}\text{O}$  energy with inclusion of correlation. It takes more elaborate way than shifting the overall  $p$ - $sd$ -shell gap. The PSDMOD interaction was modified so that the energies of the  $1/2^-$  and  $3/2^-$  of  $^{15}\text{O}$ , the  $5/2^+$ ,  $1/2^+$ , and  $3/2^+$  of  $^{17}\text{O}$ , the  $0^+$  of  $^{12}\text{C}$ , and the  $0^+$  of  $^{20}\text{Ne}$  measured from the ground state of  $^{16}\text{O}$  were exactly reproduced [16]. The second model space is the Zuker-Buck-McGrory ( $z\text{bme}$ ) model space [17], which is adopted for negative parity states,  $1/2^-$  3.055 MeV,  $1/2_2^-$  5.939 MeV,  $3/2^-$  4.553 MeV,  $3/2_2^-$  5.379 MeV,  $5/2^-$  3.842 MeV,  $5/2_2^-$  5.732 MeV,  $7/2^-$  5.697 MeV,  $9/2^-$  5.215 MeV, and  $11/2^-$  7.757 MeV. For this model, the orbits  $1s_{1/2}$  and  $1p_{3/2}$  are filled (inert  $^{12}\text{C}$  nucleus core) and the active (valence) particles were restricted to  $1p_{1/2}$ ,  $2s_{1/2}$ , and  $1d_{5/3}$  orbits with the REWILE effective Hamiltonians [18]. The REWILE two-body effective Hamiltonian was specified by 30 two-body matrix elements (TBMEs). The one-body part of the Hamiltonian is specified by three single-particle energies, which in this model are interpreted as the binding energies of particles in the three active orbits to the assumed inert  $^{12}\text{C}$  core. These 33 matrix elements were treated as free parameters in the least-squares fit of SM eigenvalues to 19 ground state binding energies and 134 excitation energies of selected levels in nuclei with  $A = 13-22$  [19].

It would be an interesting advance to unify the interactions used for HF calculations of closed-shell nuclei with those used for the valence spectra. One of the most successful and commonly used phenomenological interactions for HF calculations is the zero-range density-dependent Skyrme-type interaction. So, for all excited states, Skyrme interactions are adopted to generate from them a one-body potential in Hartree-Fock theory to calculate the single-particle matrix elements. The single-particle matrix elements are calculated with the Skyrme-Hartree-Fock (SHF) potential with two different parametrizations in addition to realistic Wood-Saxon (WS) and harmonic oscillator (HO) potentials for comparison. The

SHF is a mean-field (MF) potential. The essential aspect of the MF method is that for a given two-body interaction, the energy of a single Slater determinant is minimized [19]. For a spherical basis, the Skyrme interaction provides an analytic energy density functional which can be computationally solved very quickly in order to give the minimum energy, the self-consistent potential, and single-particle densities. The MF can also be carried out in a deformed or general basis.

## II. THEORY AND METHODOLOGY

The reduced matrix element of the electron scattering operator for an  $n$ -particle model space wave function of multipolarity  $\lambda$  is expressed as the sum of the product over the one-body density matrix (OBDM) elements times reduced single-particle matrix elements, and is given by [20]

$$\begin{aligned} \langle f \| \hat{O}^\lambda \| i \rangle &= \langle n\omega_f J_f \| \hat{O}^\lambda \| n\omega_i J_i \rangle \\ &= \sum_{k_\alpha k_\beta} \text{OBDM}(f i k_\alpha k_\beta \lambda) \langle k_\alpha \| \hat{O}^\lambda \| k_\beta \rangle, \end{aligned} \quad (1)$$

where  $k$  stands for the single-particle states ( $n l j$ ) and  $i$  and  $f$  labels are a shorthand notation for the initial and final model space states,  $(n\omega_i J_i)$  and  $(n\omega_f J_f)$ , respectively. The  $\omega$  indices distinguish the various basis states with the same  $J$  value. The OBDM in the proton-neutron formalism is given by [20]

$$\text{OBDM}(f i k_{\alpha,t_z} k_{\beta,t_z} \lambda) = \frac{\langle n\omega_f J_f \| [a_{k_{\alpha,t_z}}^+ \otimes \tilde{a}_{k_{\beta,t_z}}]^\lambda \| n\omega_i J_i \rangle}{\sqrt{2\lambda + 1}}, \quad (2)$$

where  $t_z = 1/2$  for a neutron and  $t_z = -1/2$  for a proton.

For the central potential, we use the Skyrme potential; it is a two-body interaction. One may generate from it a one-body potential in Hartree-Fock theory, as in the codes used. It is supposed to provide the mean field due to all the nucleons which compose the nucleus, and approximates the realistic nucleon-nucleon (and nucleon-nucleon-nucleon) forces. The Skyrme potential  $V_{\text{Skyrme}}$  can be written as [21]

$$\begin{aligned} V_{\text{Skyrme}}(\vec{r}_1, \vec{r}_2) &= t_0(1 + x_0 \hat{P}_\sigma) \delta_{12} + \frac{t_1}{2}(1 + x_1 \hat{P}_\sigma) [\vec{k}'^2 \delta_{12} + \delta_{12} \vec{k}^2] \\ &+ t_2(1 + x_2 \hat{P}_\sigma) \vec{k}' \delta_{12} \vec{k} \\ &+ \frac{t_3}{6}(1 + x_3 \hat{P}_\sigma) \rho \left( \frac{\vec{r}_1 + \vec{r}_2}{2} \right)^\alpha \delta_{12} \\ &+ i W_0 \vec{k}' \delta_{12} (\hat{\sigma}_1 + \hat{\sigma}_2) \times \vec{k} \\ &+ \frac{t_e}{2} [3(\hat{\sigma}_1 \cdot \vec{k}')(\hat{\sigma}_2 \cdot \vec{k}') - (\hat{\sigma}_1 \cdot \hat{\sigma}_2) \vec{k}'^2] \delta_{12} \\ &+ \delta_{12} [3(\hat{\sigma}_1 \cdot \vec{k})(\hat{\sigma}_2 \cdot \vec{k}) - (\hat{\sigma}_1 \cdot \hat{\sigma}_2) \vec{k}^2] \\ &+ t_0 [3(\hat{\sigma}_1 \cdot \vec{k}) \delta_{12} (\hat{\sigma}_2 \cdot \vec{k}) - (\hat{\sigma}_1 \cdot \hat{\sigma}_2) \vec{k}' \delta_{12} \vec{k}], \end{aligned} \quad (3)$$

where

$$\delta_{12} = \delta(\vec{r}_1 - \vec{r}_2) \quad (4)$$

and

$$\hat{k} = \frac{1}{2i}(\vec{\nabla}_1 - \vec{\nabla}_2), \quad \hat{k}' = -\frac{1}{2i}(\vec{\nabla}_1 - \vec{\nabla}_2), \quad (5)$$

which are the relative momentum operators which operate on the wave functions to the right and to the left.  $\hat{P}_\sigma$  is the

spin-exchange operator given by

$$\hat{P}_\sigma = \frac{1}{2}(1 + \hat{\sigma}_1 \cdot \hat{\sigma}_2). \quad (6)$$

The momentum-dependent terms are introduced to take into account the effect of the finite-range force and are important for the surface properties [22].

In the present calculations, two Skyrme parametrizations, SLy4 [23] and SkXcsb [24], are implemented. These parametrizations give a good reproduction of the binding energy as well as the root-mean-square (rms) radii. In SLy4, the pairing correlations are included using a density dependent zero-range force. The SkXcsb includes charge symmetry breaking (CSB) in the  $s$ -wave part of the Skyrme interaction together with the usual Coulomb direct (CD) and exchange (CE) terms. The direct Coulomb potential is obtained by folding the calculated charge distribution,  $\rho_{\text{ch}}(r)$ , with the two-body Coulomb interaction, and is given by [25]

$$H_{\text{CD}} = \frac{e^2}{2} \int_0^\infty \int_0^\infty \frac{\rho_p(r)\rho_p(r')}{|r-r'|} d^3r d^3r'. \quad (7)$$

The exchange part of the Coulomb interaction comes from the Slater approximation, and is the first term of the density matrix expansion in the local density approximation; it is given by

$$H_{\text{CE}} = -\frac{3}{4} e^2 \left(\frac{3}{\pi}\right)^{1/3} \int_0^\infty \rho_p(r)^{4/3} d^3r \quad (8)$$

Longitudinal (Coulomb) electron scattering form factors for inelastic scattering between an initial ( $i$ ) and final ( $f$ ) state or, for elastic scattering ( $i = f$ ), are denoted by  $F(C\lambda, q, f, i)$ . The transverse electric and transverse magnetic form factors are denoted by  $F(E\lambda, q, f, i)$  and  $F(M\lambda, q, f, i)$ , respectively, where  $\lambda$  is the multipolarity [26]. The last two types of form factors can be divided into components according to the convection currents  $\lambda c$  (due to the orbital motion of the nucleons) and the magnetization currents  $\lambda m$  (due to the intrinsic magnetic moments of the nucleons) [27]:

$$F(E\lambda, q, f, i) = F(E\lambda c, q, f, i) + F(E\lambda m, q, f, i), \quad (9)$$

$$F(M\lambda, q, f, i) = F(M\lambda c, q, f, i) + F(M\lambda m, q, f, i). \quad (10)$$

So we can write the total longitudinal form factor as

$$|F_C(q, f, i)|^2 = \sum_{\lambda \geq 0} |F(C\lambda, q, i, f)|^2 \quad (11)$$

and the total transverse form factor as

$$|F_T(q, f, i)|^2 = \sum_{\lambda > 0} \{|F(E\lambda, q, i, f)|^2 + |F(M\lambda, q, i, f)|^2\}. \quad (12)$$

Electron scattering form factors involving angular momentum  $\lambda$  and momentum transfer  $q$ , between initial and final

nuclear SM states of spin  $J_{i,f}$ , are given by [27]

$$|F(X\lambda, q, f, i)|^2 = N_p \left| \sum_{t_z} \langle n\omega_f J_f || \hat{O}^\lambda(X, q, t_z) || n\omega_i J_i \rangle \right|^2 \times F_{\text{cm}}^2(q) F_{fs}^2(q), \quad (13)$$

where  $N_p = 4\pi/Z^2(2J_i + 1)$ , and the variable  $X$  selects the longitudinal ( $L$  or  $C$ ) and transverse ( $T$ ) form factors. Some of the most important nuclear physics information is contained in these two form factors.

$F_{\text{cm}}(q)$  is the correction for the lack of translational invariance in the SM (center-of-mass correction) and  $F_{fs}(q)$  is the nucleon finite size ( $fs$ ) form factor.

The total form factor is the sum of the longitudinal and transverse terms:

$$|F(q)|^2 = |F_C(q, f, i)|^2 + [1/2 + \tan^2(\theta/2)] |F_T(q, f, i)|^2, \quad (14)$$

where  $\theta$  is the electron scattering angle.

The reduced transition probability is given by [20]

$$B(X\lambda) = \frac{Z^2}{4\pi} \left[ \frac{(2\lambda + 1)!!}{k^\lambda} \right]^2 |F(X\lambda, k)|^2, \quad (15)$$

where  $k = E_x/\hbar c$ .

$B(M1)$  is in units of  $u_N^2$ ,  $B(E2)$  is in units of  $e^2\text{fm}^4$ ,  $B(M2)$  is in units of  $u_N^2\text{fm}^2$ , and  $B(E1)$  is in units of  $e^2\text{fm}^2$ , where  $u_N$  is the nuclear magneton  $u_N = \frac{e\hbar}{2m_p c} = 0.1051 \text{ efm}$

### III. RESULTS AND DISCUSSION

In the present work, the OBDM elements are calculated using the SM code NUSHELLX@MSU [28]. NUSHELLX@MSU is a set of wrapper codes written by Alex Brown that use data files for model spaces and Hamiltonians to generate input for NUSHELLX. NUSHELLX is a set of computer codes written by Bill Rae [29] that are used to obtain exact energies, eigenvectors, and spectroscopic overlaps for low-lying states in shell model Hamiltonian matrix calculations with very large basis dimensions. It uses a  $J$ -coupled proton-neutron basis, and  $J$ -scheme matrix dimensions of up to the order of 100 million can be considered. The wrapper codes also convert the NUSHELLX output into figures and tables for energy levels, gamma decay, and beta decay. The OBDM elements are then used to calculate the matrix elements of  $C\lambda$ ,  $E\lambda$ , and  $M\lambda$  operators. As we mentioned previously, in all our calculations, the radial wave functions of the single-particle matrix elements are calculated using a two-body Skyrme interaction potential, from which a one-body potential in Hartree-Fock theory of types SLy4 and SkXcsb can be generated. These parametrizations give the rms charge radii equal to 2.786 and 2.739 fm, respectively, in a good agreement with the experimental value 2.6932 fm [30]. Also, the calculated total binding energies are 134.37 and 133.163 MeV, respectively, which are in good agreement with the experimental value 131.765 MeV [5]. Furthermore, the calculations with Skyrme parametrizations are compared with those of the HO and WS single-particle potentials. The oscillator size parameter  $b = 1.747 \text{ fm}$  chosen to reproduce the

TABLE I. rms radii (fm) for  $^{17}\text{O}$  nucleus using different single-particle potentials.

| Potential | Proton | Neutron | Mass  | Charge | Charge expt. [30] |
|-----------|--------|---------|-------|--------|-------------------|
| SLy4      | 2.717  | 2.787   | 2.754 | 2.786  | 2.6932            |
| SkXcsb    | 2.669  | 2.731   | 2.702 | 2.739  |                   |
| HO        | 2.620  | 2.700   | 2.663 | 2.693  |                   |
| WS        | 2.653  | 2.718   | 2.688 | 2.724  |                   |

measured rms charge radius. For all electric transitions ( $\lambda > 0$ ), the standard effective charges with  $e_p = 1.5e$  and  $e_n = 0.5e$  are used, using the Tassie model for core polarization [31]. For magnetic transitions, free  $g$  factors are used.

The calculated proton, neutron, mass, and charge radii for  $^{17}\text{O}$  using different single-particle potentials are given in Table I along with the experimental data [30]. The agreement with the experimental values is seen to be good.

Discussion of the results will be divided into two parts. The first one pertains to the elastic electron scattering form factors. The second one is related to the inelastic electron scattering form factors, energy levels, and transition probabilities for (i) positive parity states ordered according to increasing angular momentum and (ii) the corresponding negative parity states.

### A. Elastic electron scattering form factors ( $J^\pi = 5/2^+$ )

The ground-state spin and parity assignment for  $^{17}\text{O}$  is  $5/2^+$ . Thus, in elastic scattering the allowed longitudinal multipoles are  $C0$ ,  $C2$ , and  $C4$ , and the transverse multipoles are  $M1$ ,  $M3$ , and  $M5$ . The contributions of these multipoles are calculated using the full  $psdpm$  model space with the PSDMOD two-body effective interaction [16] with SkXcsb parametrization and are depicted in Figs. 1(a) and 1(b). From this figure, it can be seen that the total longitudinal form factor is dominated by the contribution of  $C0$  in the low momentum transfer region, and shows further diffraction structures at higher  $q$ . The elastic

transverse magnetic electron scattering experimental data for  $^{17}\text{O}$  are available from Ref. [32], covering a momentum transfer region up to  $q = 2.8 \text{ fm}^{-1}$ . A comparison of the present results with experimental data is made in order to account for the effects of the variation of the single-particle potentials. From this figure, it is obvious that the total magnetic form factor is dominated by the contribution of  $M1$  effects in the low momentum transfer region. In the intermediate region, the  $M3$  contribution has the dominant effect on the calculated total form factor, whereas it was confirmed experimentally that the  $M3$  part is strongly depressed in the experimental data. In this region, the discrepancy with the experimental data can be reduced by hindering the  $M3$  part by using core polarization.

At high momentum transfer, the main contribution to the total form factor is coming from the  $M5$  values. Generally, the calculated total transverse magnetic form factor is broadly consistent with the major trends of the experimental data.

In order to determine the sensitivity of the elastic electron scattering form factors with the variation of the single particle potentials, the total elastic transverse magnetic form factors are calculated using the full  $psdpm$  model space with SLy4, SkXcsb parametrizations, HO, and WS, and they are presented in Fig. 2 along with the available experimental data. A similar hindrance of the  $M3$  form factor is observed. Also, it illustrates that the best potential for reproducing the experimental data is SkXcsb.

### B. Inelastic electron scattering form factors

#### 1. Positive parity states

In all selected positive parity states, the  $psdpm$  SM space with the PSDMOD two-body effective interaction [16] is used in reproducing the longitudinal and transverse electron scattering form factor profiles.

Inelastic longitudinal Coulomb  $C2$  form factors for the first  $1/2^+$  state of the  $^{17}\text{O}$  nucleus at 0.870 MeV are shown in Fig. 3(a). Comparison is made with the available experimental

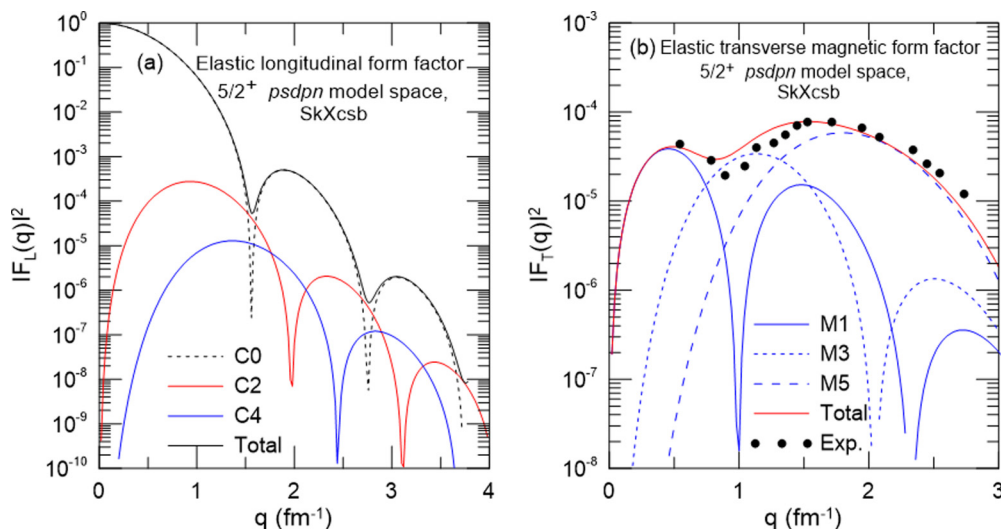


FIG. 1. Theoretical elastic longitudinal (a) and transverse (b) form factors for  $5/2^+$ , and their multipole contributions using SkXcsb parametrization, compared with the experimental data taken from Ref. [32].

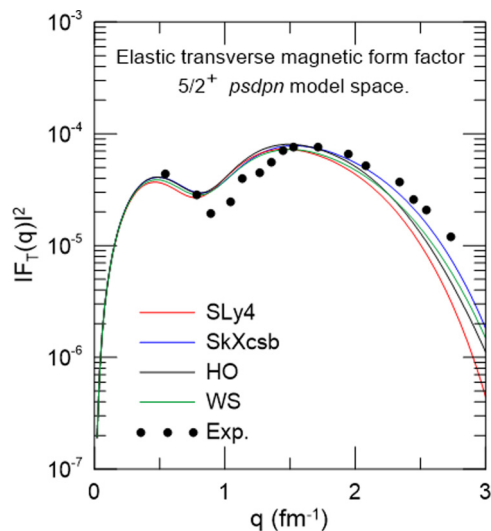


FIG. 2. Theoretical elastic transverse form factors for  $5/2^+$ , using SLy4, SkXcsb parametrizations, HO, and WS compared with the experimental data taken from Ref. [32].

data taken from Ref. [10]. It can be seen that the SHF (solid and dashed curves) results are in a good agreement with the experimental data within the experimental errors in all regions of momentum transfer. Also, HO and Woods-Saxon results agree with the experimental data. The transverse form factors are shown in Fig. 3(b). Both  $E2$  and  $M3$  multipoles contribute to the transverse form factor as shown in Fig. 3(c). This behavior is evidence for the collective components in their wave functions.

To establish the reliability of SHF implementation with SM, the form factors for some higher-lying states are calculated in the present work. In these states, the longitudinal multipoles are generally predicted to be dominant. For this purpose, the longitudinal  $C2$  form factor for the states at  $1/2_2^+$ , 6.356 MeV and  $1/2_3^+$ , 7.956 MeV are plotted in Figs. 4(a) and 4(b). In comparisons with available experimental data, it is clear that the predicted form factors are in reasonable agreement with the experimental data.

The total longitudinal form factors for the  $3/2^+$ , 5.084 MeV state are shown in Fig. 5(a). The predicted total form factors are compared with the experimental data. Inspection of these curves reveals that the *psdnp* predictions with Skyrme parametrizations and WS potential exhibit qualitative similarity to the shape of the experimental data, although they considerably overestimate its magnitude. The radial single-particle wave functions from the self-consistent mean field code that we use are optimal for hole states, but not necessarily so for particle states. Hence, excited states containing large contributions from particle states may give unreliable form factors. Likewise, the shell model code is optimal for spectroscopic properties, not necessarily so for the nuclear charge density. It seems that the core polarization effects with polarization charge  $0.5e$  give a large contribution for Skyrme and WS potentials, but not for the HO oscillator potential, which gives a good description of

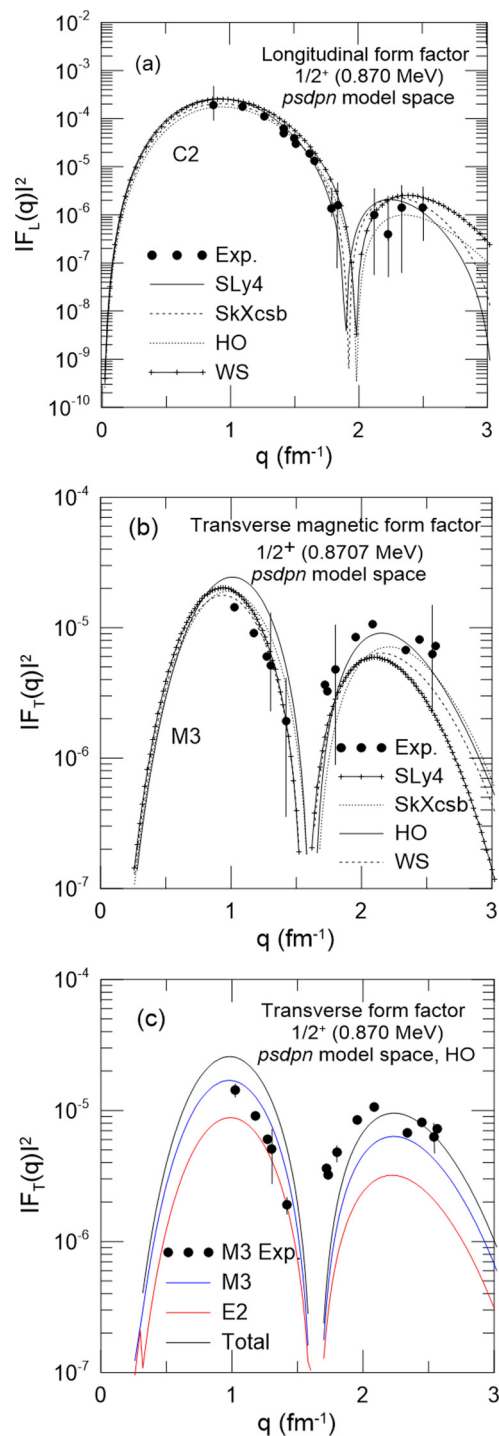


FIG. 3. Theoretical longitudinal (a) and transverse (b) form factors for the  $1/2^+$ , 0.870 MeV state using SLy4, SkXcsb parametrizations, HO, and WS compared with the experimental data taken from Ref. [10]. The  $E2$  and  $M3$  multipole contributions are shown for the HO potential (c).

the data. The  $C2$  and  $C4$  multipole contributions shown in this figure are for the HO potential.

Encouraged by the reasonable agreement between the calculated longitudinal form factor using the HO single-particle

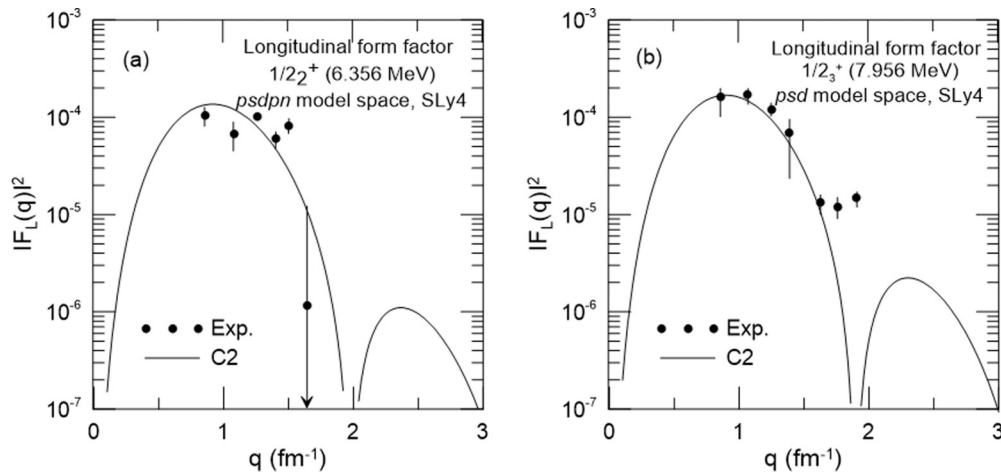


FIG. 4. Theoretical longitudinal  $C2$  form factors using SLy4 parameterization for the (a)  $1/2_2^+$ , 6.356 MeV state and (b)  $1/2_3^+$ , 7.956 MeV state compared with the experimental data taken from Ref. [10].

potential with experimental data in  $3/2^+$  state, we use this potential to calculate the total transverse form factor and its mixed multiplicities  $M1$ ,  $E2$ ,  $M3$ , and  $E4$ . As shown in Fig. 5(b), the  $psdnp$  predictions with HO wave functions overestimate the measured transverse form factor. This behavior is additional evidence for collective components in their wave functions. As stated above, the shell model code is optimal for spectroscopic properties, not necessarily so for the convection and magnetization current densities. Also, core polarization effects are not considered for transverse form factors.

Due to the reasonable agreement between the calculated longitudinal form factor using the HO single-particle potential with the experimental data in the  $3/2_1^+$  state, we use this potential to calculate the longitudinal  $C2$  form factor for the  $3/2_2^+$  state with an excitation energy of 5.869 MeV, as shown in Fig. 6. The HO single-particle potential for this state gives a remarkable agreement with the available experimental data [10].

The longitudinal  $C0$  and  $C2$  electron scattering form factors for the  $5/2^+$ , 6.862 MeV state are shown in Fig. 7. It is

obvious that the shape of the experimental form factor is well described by the  $psdnp$  model space using the four potentials, although a slight deviation exists. In the light of the best agreement in Fig. 7, the SLy4 parametrization is selected to calculate the longitudinal  $C2$  form factor for the  $5/2_3^+$ , 8.402 MeV transition, and it is plotted in Fig. 8 together with the existing experimental data. The  $q$  dependence of the calculated form factor for this transition indicates that the experimental data falls off slightly less rapidly than those of the SLy4 parametrization.

Inelastic longitudinal  $C2$  form factor for the  $7/2^+$ , 7.576 MeV state is shown in Fig. 9. Inspection of these curves reveals that the  $psdnp$  predictions with all selected single-particle potentials do not yield an adequate description of the experimental data for the momentum transfer region below  $q = 1.4 \text{ fm}^{-1}$ . Beyond this region, the  $psdnp$  prediction reproduces more precisely the experimental data.

Finally, inelastic longitudinal  $C2$  form factors for the first observed level of  $9/2^+$ , 8.470 MeV are shown in Fig. 10 using

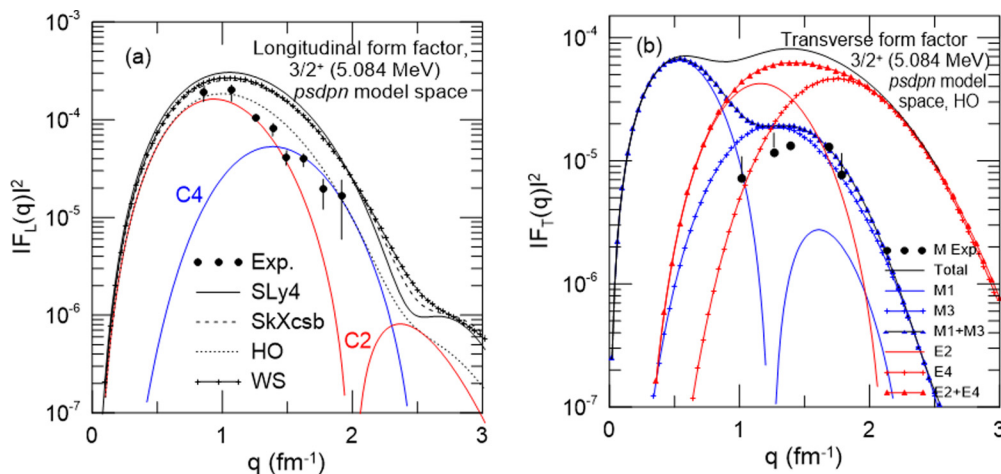


FIG. 5. Theoretical longitudinal (a) and transverse (b) form factors and their multipole contributions for  $3/2^+$ , 5.084 MeV using SLy4, SkXcsb parametrizations, HO, and WS compared with the experimental data taken from Ref. [10]. The multipole contributions are shown for the HO potential.

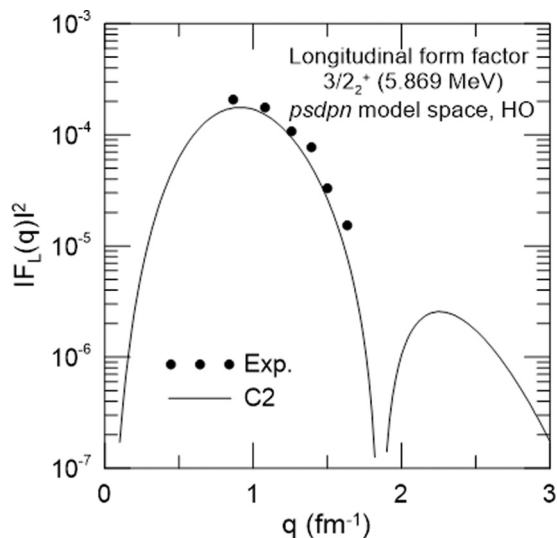


FIG. 6. Theoretical longitudinal C2 form factors using the HO potential for the  $3/2_2^+$ , 5.869 MeV state compared with the experimental data taken from Ref. [10].

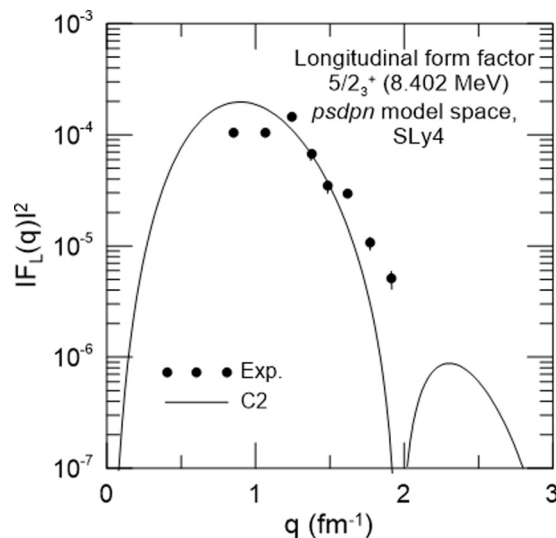


FIG. 8. Theoretical longitudinal C2 form factors using the SLy4 parametrization for the  $5/2_3^+$ , 8.402 MeV state compared with the experimental data taken from Ref. [10].

the four potentials along with the available experimental data. The available experimental data are well reproduced.

## 2. Negative parity states

The *z*bme SM space predictions of the longitudinal and transverse form factors for the first excitation of the  $1/2^-$  state, 3.055 MeV, are depicted in Figs. 11(a), 11(b), and 11(c) along with the available experimental data. The multiplicities included in this transition are pure longitudinal C3 and transverse M2 and E3. It is obvious that the shape of the calculated C3 form factor using the HO potential is

in qualitative agreement with the experimental data over all momentum transfer regions, and the agreement is better than that of other selected potentials. Also, it can be noticed that the *z*bme prediction for the transverse M2 form factors exceed the corresponding experimental data. The deviation decreases gradually. The consistency of *z*bme predictions for the second excitation of the  $1/2^-$  state, 5.939 MeV, is shown in Figs. 12(a) and 12(b). The experimental longitudinal C3 form factor data for this state is compared with those ones determined by using SLy4, SkXcsb, HO, and WS potentials. All results in this state are close to each other and slightly underpredict the

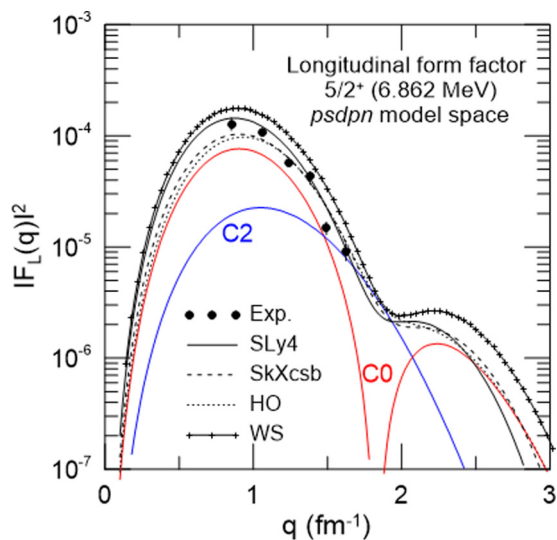


FIG. 7. Theoretical longitudinal form factors for the  $5/2_2^+$ , 6.862 MeV state using SLy4, SkXcsb parametrizations, HO, and WS compared with the experimental data taken from Ref. [10]. Multipole contributions are shown for the SLy4 parametrization.

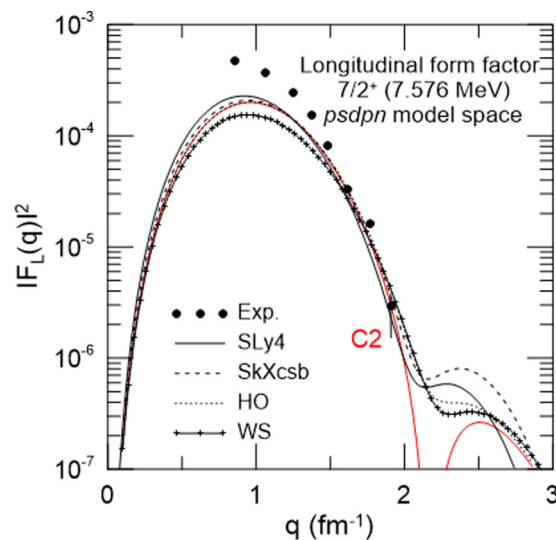


FIG. 9. Theoretical longitudinal form factors for the  $7/2_2^+$ , 7.576 MeV state using SLy4, SkXcsb parametrizations, HO, and WS compared with the experimental data taken from Ref. [10]. Multipole contributions are shown for the SLy4 parametrization.

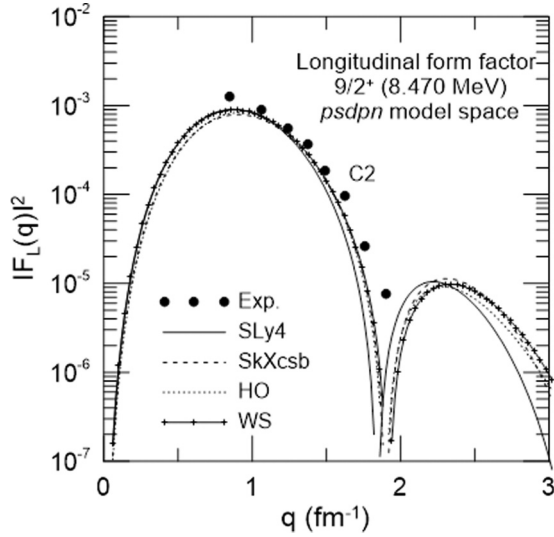


FIG. 10. Theoretical longitudinal form factors and their multipole contributions for the  $9/2^+$ , 8.470 MeV state using SLy4, SkXcbsb parametrizations, HO, and WS compared with the experimental data taken from Ref. [10].

experimental data. Figure 11(b) illustrates the transverse form factor for the same state and the multipole contributions using SLy4 parametrization in comparison with the experimental data. From this figure, it can be seen that the transverse form factor is ascribed mainly to the  $M2$  transition and is in reasonable agreement with the experimental data.

The measured longitudinal form factors for the first observed  $3/2^-$  state at 4.553 MeV is depicted in Fig. 13 in comparison with the predictions of the corresponding *zbme*. The individual multipoles for this transition,  $C1$  and  $C3$ , calculated with SLy4 parametrization are also shown. It is obvious from Fig. 13 that the *zbme* prediction readily shows a rapid increase in the low-lying  $C3$  strength. This, of course, means that it is the  $^{16}\text{O}$  core excitations that are responsible for the considerable  $C3$  strength. The longitudinal form factor extracted for the  $3/2^-$ , 5.379 MeV state and its individual multipoles are shown in Fig. 14 along with experimental data. As can be seen from this figure, the *zbme* prediction is in general agreement with the experimental data for all observed  $q$  dependence regions.

In Fig. 15 the experimental longitudinal form factor for the first  $5/2^-$  state at 3.842 MeV is compared to the *zbme* predictions, which clearly gives another indication of a  $C3$  strength. The observed momentum transfer dependence is consistent with the theory, although a notable aspect is the extent to which the *zbme* predictions underestimate the experimental data. Figure 16 shows the longitudinal form factor for the first  $5/2^-$  state at 5.732 MeV. In this state, a longitudinal form factor is dominated by a  $C3$  component and there is no measurable  $C1$  component [10]. The consistency of the *zbme* predictions is seen to be good and the shape agrees well with experimental data, but the magnitude is underestimated.

Figure 17 shows the longitudinal form factors for the first observed  $7/2^-$  state at 5.697 MeV. The consistency of the

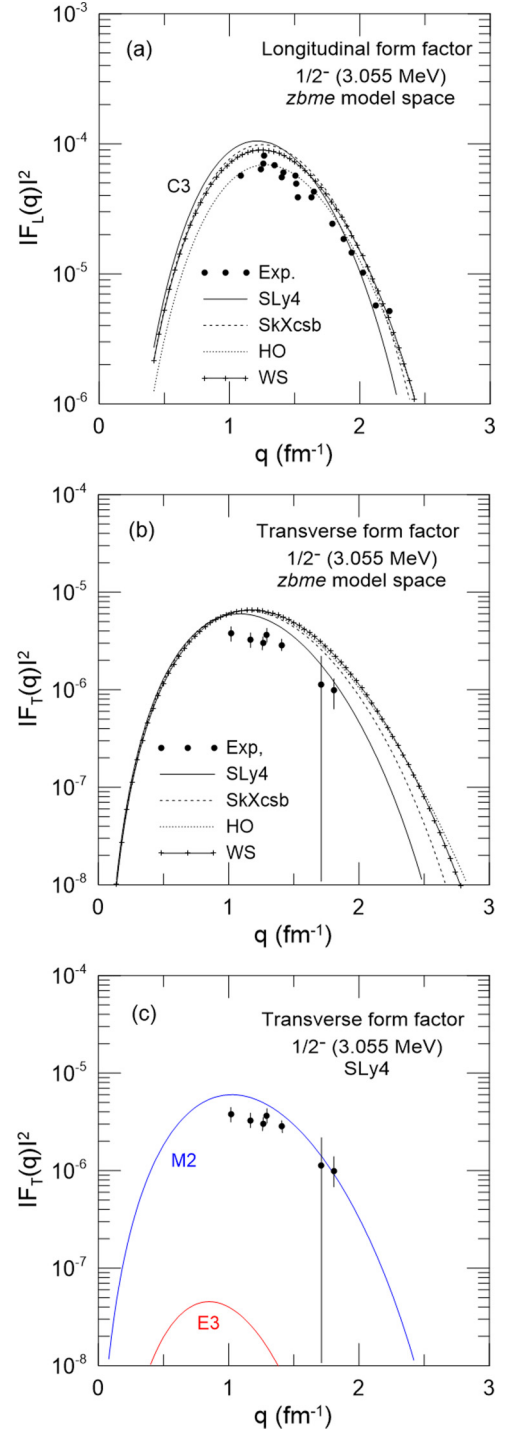


FIG. 11. Theoretical longitudinal (a) and transverse (b) form factors for the  $1/2^-$ , 3.055 MeV state using SLy4, SkXcbsb parametrizations, HO, and WS compared with the experimental data taken from Ref. [10].  $M2$  and  $E3$  multipole contributions for the SLy4 parametrization are shown in (c).

experimental data with those obtained using the four potentials is seen to be excellent. Furthermore, the shapes exhibit that the  $C1$  component has a dominant contribution to the total form factor in a low momentum transfer region up to  $q = 1 \text{ fm}^{-1}$ ,



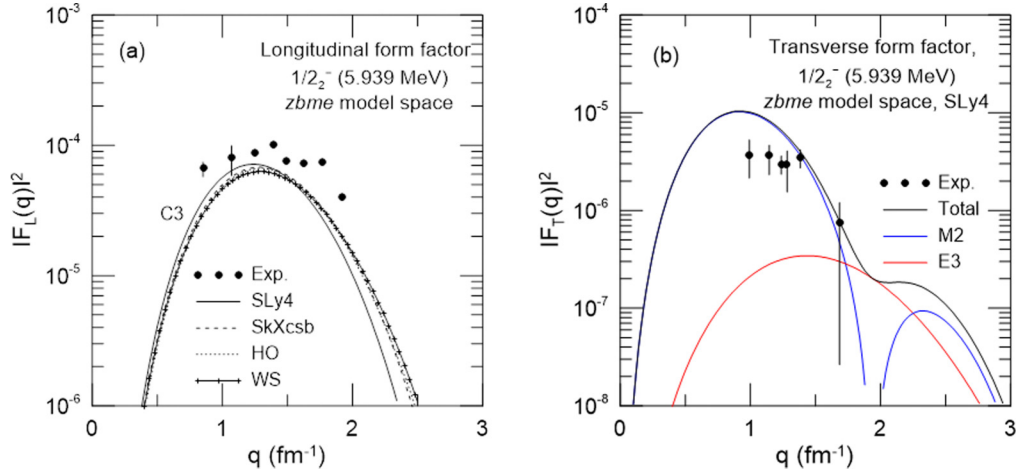


FIG. 12. Theoretical longitudinal (a) form factors for the  $1/2^-$ , 5.939 MeV state using SLy4, SkXcsb parametrizations, HO, and WS compared with the experimental data taken from Ref. [10]. Transverse form factors and their  $M2$  and  $E3$  multipole contributions calculated with the SLy4 parametrization are shown in (b) in comparison with the experimental data of Ref. [10].

whereas the  $C3$  component is dominant within the momentum transfer range from 0.4 to  $2.5 \text{ fm}^{-1}$ .

The first state with  $9/2^-$  spin-parity assignments is identified in  $^{17}\text{O}$  at 5.215 MeV. The experimental longitudinal form factor and  $z\text{bme}$  predictions are shown in Fig. 18. In this state only the  $C3$  component should contribute noticeably to the longitudinal form factor. It is obvious that the predictions are in reasonable agreement, failing only in falling below the experimental data at high  $q$  values.

Finally, the experimental longitudinal form factor of the first observed  $11/2^-$  state at 7.757 MeV is shown in Fig. 19 in comparison with the corresponding  $z\text{bme}$  predictions. Inspection of these curves reveals that the predictions are in good overall

agreement with the global aspects of the experimental data. Furthermore, the  $z\text{bme}$  prediction reproduces more precisely the experimental data at high  $q$  values with HO and WS than with Skyrme potentials.

### C. Energy level and reduced transition probabilities

The energy levels for low-lying and some second and third sequences of positive and negative parity states in  $^{17}\text{O}$  are calculated in the  $psdpn$  and  $z\text{bme}$  SM spaces without using any restrictions with PSDMOD and REWILE two-body effective interactions. Concerning the comparison with the experimental energy levels [5], Fig. 20 depicts the calculated energy level

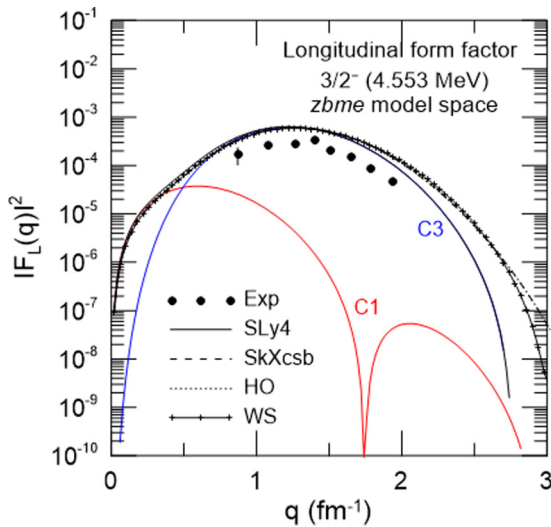


FIG. 13. Theoretical longitudinal form factors for the  $3/2^-$ , 4.553 MeV state using SLy4, SkXcsb parametrizations, HO, and WS compared with the experimental data taken from Ref. [10]. Multipole contributions are shown for the SLy4 parametrization.

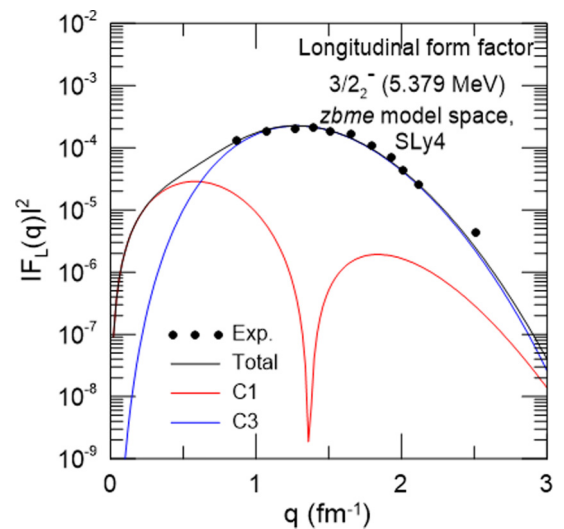


FIG. 14. Theoretical longitudinal form factors and their multipole contributions for  $3/2^-$ , 5.379 MeV using the SLy4 parametrization compared with the experimental data taken from Ref. [10].

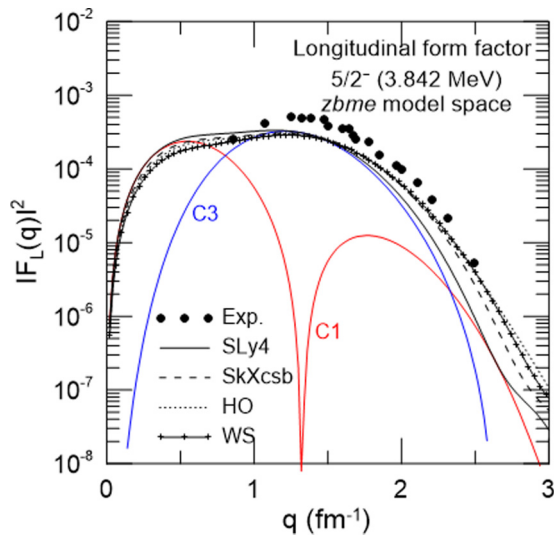


FIG. 15. Theoretical longitudinal form factors for  $5/2^-$ , 3.84 MeV using SLy4, SkXcsb parametrizations, HO, and WS compared with the experimental data taken from Ref. [10]. Multipole contributions are shown for the SLy4 parametrization.

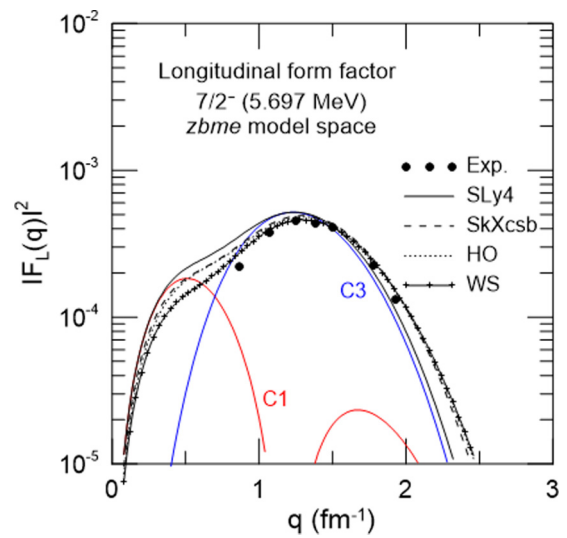


FIG. 17. Theoretical longitudinal form factors for the  $7/2^-$ , 5.697 MeV state using SLy4, SkXcsb parametrizations, HO, and WS compared with the experimental data taken from Ref. [10]. Multipole contributions are shown for the SLy4 parametrization.

schemes in comparison with the experimental data taken from Ref. [5]. The spectrum is shown by energy levels (lines); blue and red lines are for positive and negative parity states, respectively. From Fig. 20, it is clear that most of the calculated excitation energies in the *psdnpn* model space agree reasonably well with the experimental data, on the whole, except for a few levels. Those levels for which the discrepancies are larger than 1 MeV are the first excited  $1/2^-$  level at 3.055 MeV, the first excited  $5/2^-$  level at 3.842 MeV, and first excited  $3/2^-$  level at 4.553 MeV. These discrepancies may be attributed to the coupling between the states, for instance the  $1p_{1/2}$  holes coupled to the  $1d_{5/2}$  neutron. In the *zbme* model space, the

energy levels are well predicted, but most the energy levels are below the experimental data.

The deduced transition probabilities  $B(E2 \uparrow)$  and  $B(E3 \uparrow)$  for the considered transitions in  $^{17}\text{O}$  have been tabulated in Tables II and III, respectively. Inspection of these values reveals that the most of the  $E2$  transitions agree reasonably well with the experimental ones. In general, present calculated  $E2$  transition rates are slightly smaller than the experimental data except for  $J^\pi = 1/2^+$ , where the agreement is quite good. The slight deviation with the experimental data may be due to neglecting the quadrupole vibration. Regarding  $E3$  transition

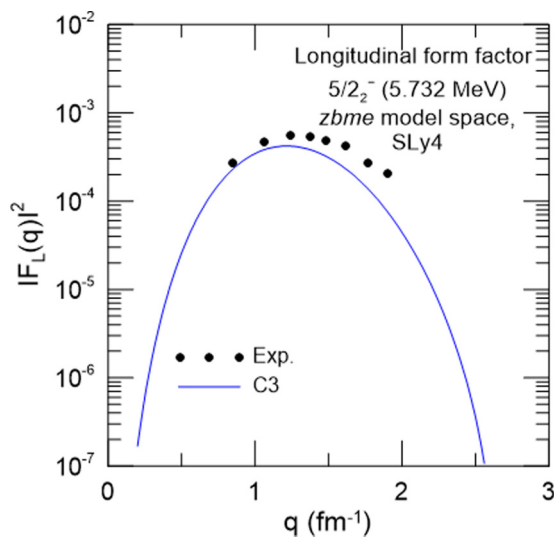


FIG. 16. Theoretical longitudinal C3 form factors for the  $5/2^-$ , 5.732 MeV state using the SLy4 parametrization compared with the experimental data taken from Ref. [10].

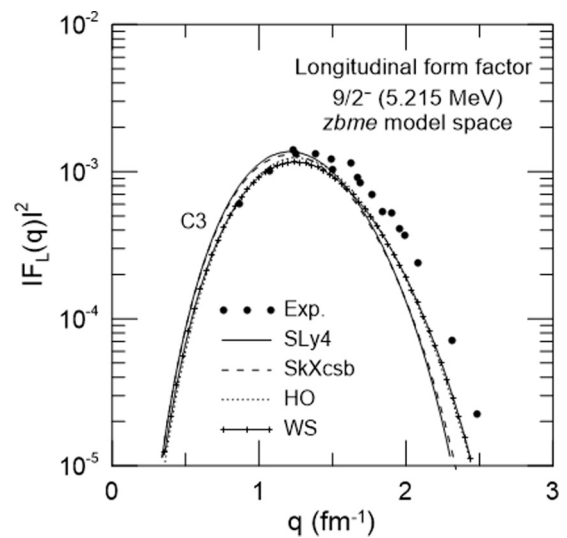


FIG. 18. Theoretical longitudinal form factors for the  $9/2^-$ , 5.215 MeV state using SLy4, SkXcsb parametrizations, HO, and WS compared with the experimental data taken from Ref. [10].

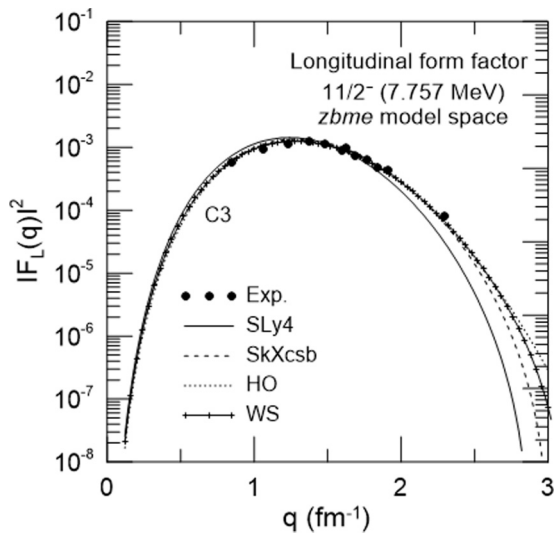


FIG. 19. Theoretical longitudinal form factors for the  $11/2^-$  7.757 MeV state using SLy4, SkXcsb parametrizations, HO, and WS compared with the experimental data taken from Ref. [10].

probabilities, it has been found that the agreement is good for the states  $J^\pi = 3/2^-, 5/2^-, 9/2^-$ , and  $11/2^-$ , and  $B(E3 \uparrow)$  was reproduced correctly, whereas there is a slight deviation noticed in the other states. Furthermore, it is obvious that there is a rapid growth in the low-lying  $E3$  strength; this means that the  $^{16}\text{O}$  core excitations are responsible for the considerable  $E3$  strength.

TABLE II.  $B(E2 \uparrow)$  values (in  $e^2\text{fm}^4$ ) for positive parity states in  $^{17}\text{O}$ .

| $E$ (MeV) | $J^\pi$   | Present work | Experiment [10]  | Experiment [33] |
|-----------|-----------|--------------|------------------|-----------------|
| 0.8707    | $1/2^+$   | 2.1420       | $2.18 \pm 0.16$  | $2.10 \pm 0.0$  |
| 6.356     | $1/2_2^+$ | 0.3700       | $1.43 \pm 0.21$  | $2.1 \pm 1.3$   |
| 7.956     | $1/2_3^+$ | 0.4578       | $2.00 \pm 0.38$  |                 |
| 5.084     | $3/2^+$   | 0.4724       | $2.05 \pm 0.20$  | $2.5 \pm 0.7$   |
| 5.869     | $3/2_2^+$ | 1.3040       | $2.13 \pm 0.22$  |                 |
| 6.862     | $5/2^+$   | 2.9610       | $0.83 \pm 0.25$  | $1.9 \pm 1.0$   |
| 7.379     | $5/2_2^+$ | 0.1631       | 0.8              |                 |
| 7.576     | $7/2^+$   | 1.9870       | $4.20 \pm 0.51$  |                 |
| 8.47      | $9/2^+$   | 3.9010       | $10.05 \pm 1.19$ | $8.3 \pm 2.6$   |

#### IV. CONCLUSIONS

In the present work, we have continued our research into implementing the SHF with SM calculations to study the nuclear structure of the  $^{17}\text{O}$  nucleus involving both positive and negative parity states. In particular, the inelastic electroexcitation form factors in the momentum-transfer range  $0.0 < q < 3.0 \text{ fm}^{-1}$ , energy levels up to an exciting energy of 8.47 MeV, and transition probabilities have been calculated. Four single-particle potentials have been considered in this work: the Skyrme potentials (SLy4 and SkXcsb), HO, and WS. Parametrization in each potential provides a fine description of nuclear bulk properties and also of excited states of nuclei. From the outcomes of our calculations, it is possible to conclude that the reproduced charge rms, form factors, energy level scheme, and transition probabilities using the  $psdnpn$  and

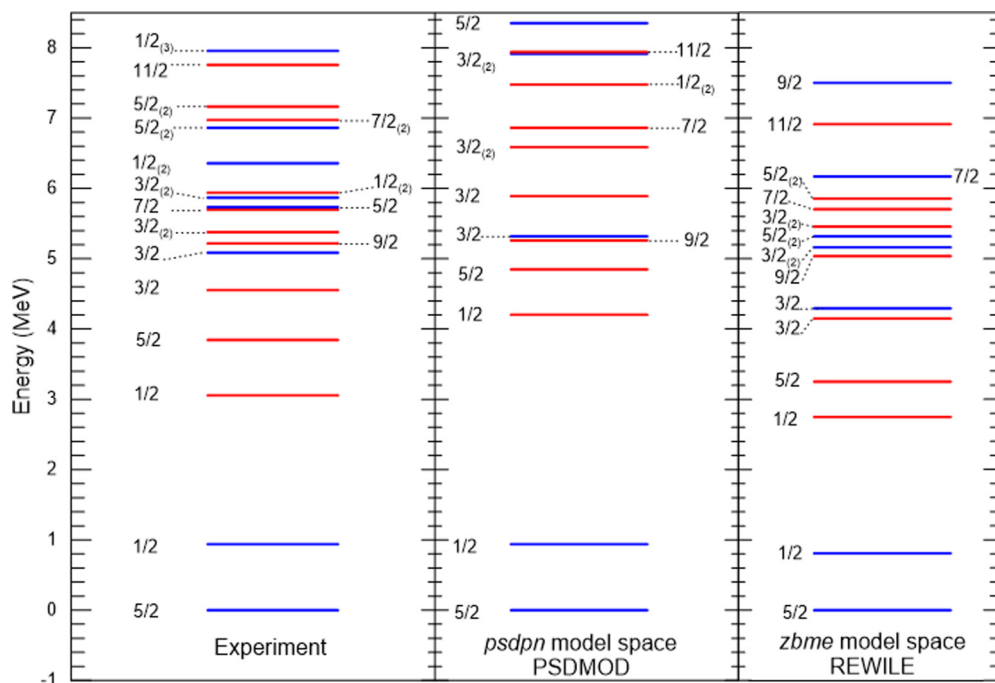


FIG. 20. Energy levels for the positive and negative parity states in  $^{17}\text{O}$  in the  $psdnpn$  and  $zbme$  SM spaces. The experimental energy levels are plotted on the left-hand side. The blue and red lines are for positive and negative parity states, respectively.

TABLE III.  $B(E3 \uparrow)$  values (in  $e^2\text{fm}^6$ ) for negative parity states in  $^{17}\text{O}$ .

| $E$ (MeV) | $J^\pi$   | Present work | Experiment [10] | Experiment [33] |
|-----------|-----------|--------------|-----------------|-----------------|
| 3.055     | $1/2^-$   | 4.382        | $14.1 \pm 3.9$  | $31.6 \pm 6$    |
| 5.939     | $1/2_2^-$ | 17.14        | $25.3 \pm 5.1$  | $17.0 \pm 10$   |
| 4.553     | $3/2^-$   | 23.73        | $20.0 \pm 12$   | $98.0 \pm 8$    |
| 3.842     | $5/2^-$   | 86.33        | $93.0 \pm 8.3$  | $153 \pm 6$     |
| 5.697     | $7/2^-$   | 127.4        | $97.0 \pm 6.5$  | $270 \pm 32$    |
| 5.215     | $9/2^-$   | 369.3        | $319.0 \pm 13$  | $360 \pm 11$    |
| 7.757     | $11/2^-$  | 339.3        | $287 \pm 14$    | $369 \pm 15$    |

$z\text{bme}$  SM spaces with SLy4 and SkXcsb parametrizations are broadly consistent with the major trends of the available experimental data, without any additional fit of parameters. It has been confirmed that combining these two methods can accommodate very well in the elastic and inelastic nuclear properties, and work better for low lying states than for higher excitations. Furthermore, the combination can be used to reproduce the positive and negative parity states after choosing the suitable model space, effective two-body interaction, and parametrization to reach highly descriptive and predictive results when investigating different nuclear configurations as well as unbound nuclei.

- [1] M. Bender, P.-H. Heenen, P.G. Reinhard, *Rev. Mod. Phys.* **75**, 121 (2003).
- [2] B. A. Brown, *Prog. Part. Nucl. Phys.* **47**, 517 (2001).
- [3] B. A. Brown and B. H. Wildenthal, *Annu. Rev. Nucl. Part. Sci.* **38**, 29 (1988).
- [4] R.A. Radhi, A. A. Alzubadi, and E. M. Rashed, *Nucl. Phys.* **947**, 12 (2016).
- [5] National Nuclear Data Center (NNDC), <http://www.nndc.bnl.gov/>
- [6] A. Muller-Arnke, *Z. Phys.* **247**, 408 (1971).
- [7] R.S. Hicks, *Phys. Rev C* **25**, 695 (1982).
- [8] G. Bohannon, L. Zamick, and E. Moya de Guerra, *Nucl. Phys. A* **334**, 278 (1980).
- [9] E. J. Kim, *Phys. Lett. B* **174**, 233 (1986).
- [10] D. M. Manley, B. L. Berman, W. Bertozzi, T. N. Buti, J. M. Finn, F. W. Hersman, C. E. Hyde, M. V. Hynes, J. J. Kelly, M. A. Kovash, S. Kowalski, R. W. Lourie, B. Murdock, B. E. Norum, B. Pugh, and C. P. Sargent, *Phys. Rev C* **36**, 1700 (1987).
- [11] A. O. Gattone and J. P. Vary, *Phys. Lett. B* **219**, 22 (1989).
- [12] S. A. Coon and L. Jaqua, *Phys. Rev C* **44**, 203 (1991).
- [13] D. C. Zheng, D. W. L. Sprung, and L. Zamick, *Nucl. Phys. A* **540**, 57 (1992).
- [14] T. Siiskonen, P. O. Lipas, and J. Rikovsky, *Phys. Rev C* **60**, 034312 (1999).
- [15] R. A. Radhi, N. Khalaf, and A. A. Najim, *Nucl. Phys. A* **724**, 333 (2003).
- [16] Y. Utsuno and S. Chiba, *Phys. Rev C* **83**, 021301 (2011).
- [17] A. P. Zuker, B. Buck, and J. B. McGrory, *Phys. Rev. Lett.* **21**, 39 (1968).
- [18] B. S. Reehal and B. H. Wildenthal, *Part. Nucl.* **6**, 137 (1973).
- [19] B. A. Brown, *RIKEN Rev.* **26**, 53 (2000).
- [20] B. A. Brown, Lecture Notes in Nuclear Structure Physics, National Superconducting Cyclotron Laboratory and Department of Physics and Astronomy, Michigan State University, E. Lansing, MI 48824, 2005 (unpublished).
- [21] D. Vautherin and D. M. Brink, *Phys. Rev. C* **5**, 626 (1972).
- [22] H. Sagawa, B. A. Brown, and O. Scholten, *Phys. Lett. B* **159**, 228 (1985).
- [23] E. Chabanat, R. Bonche, R. Haensel, J. Meyer, and R. Schaeffer, *Nucl. Phys. A* **635**, 231 (1998).
- [24] B. A. Brown, W. A. Richter, and R. Lindsay, *Phys. Lett. B* **483**, 49 (2000).
- [25] J. W. Negele and D. Vautherin, *Phys. Rev. C* **5**, 1472 (1972).
- [26] T. de Forest and J. D. Walecka, *Adv. Phys.* **15**, 1 (1966).
- [27] B. A. Brown, B. H. Wildenthal, C. F. Williamson, F. N. Rad, S. Kowalski, H. Crannell, and J. T. O'Brien, *Phys. Rev. C* **32**, 1127 (1985).
- [28] B. A. Brown and W. D. M. Rae, *Nucl. Data. Sheets* **120**, 115 (2014).
- [29] W. D. M. Rae, NuShellX, <http://www.garsington.eclipse.co.uk>
- [30] I. Angeli, *At. Data Nucl. Data Tables* **99**, 69 (2013).
- [31] B. A. Brown, R. A. Radhi, and B.H. Wildenthal, *Phys. Rep.* **101**, 313 (1983).
- [32] M. V. Hynes, H. Miska, B. Norum, W. Bertozzi, S. Kowalski, F. N. Rad, C. P. Sargent, T. Sasanuma, W. Turchinets, and B. L. Herman, *Phys. Rev. Lett.* **42**, 1444 (1979).
- [33] J. C. Kim, R. Yen, I. P. Auer, and H. S. Caplan, *Phys. Lett. B* **57**, 341 (1975).